JOURNAL OF GEOPHYSICAL RESEARCH, VOL. 91, NO. A8, PAGES 8756-8770, AUGUST 1, 1986

ALTITUDE VARIATION OF EUV EMISSIONS AND EVIDENCE FOR PROTON PRECIPITATION AT LOW LATITUDES IN THE SATURNIAN ATMOSPHERE

R. V. Yelle, B. R. Sandel, D. E. Shemansky, and S. Kumar

Lunar and Planetary Laboratory, University of Arizona, Tucson

Abstract. Extreme ultraviolet observations of Saturn from Voyager 1 and 2 are analyzed. The Lyman alpha and H_2 band emissions extend throughout the upper atmosphere, from the hydrocarbon homopause to well above the exobase. Analysis of the Lyman alpha emissions with a radiative transfer model indicates that the Lyman alpha source temperature is very high. This suggests that energetic protons or hydrogen atoms are responsible for a fraction of the emissions. Calculation of the solar-scattered component of the emissions based on the neutral atmosphere of Smith et al. (1983) reveals that only 1-2 kR out of a total of 3.5 kR of the observed Lyman alpha intensity is due to solar scatter for the Voyager 2 disc observations; the remainder of the Lyman alpha emissions are collisionally excited. The Lyman alpha and H_2 bands are constant in longitude but decrease in local time by a factor of 2 from dawn to dusk. This correlation of the Lyman alpha and H_2 band intensities is further evidence that most of the Lyman alpha is collisionally excited.

1. Introduction

The ultraviolet spectra of Jupiter and Saturn reflect the composition of their upper atmospheres: The dominant emissions are from molecular and atomic hydrogen; the only other identified emitter is helium. One of the interesting features of these emissions is that they imply an energy deposition in the upper atmosphere much greater than that deposited by solar EUV radiation [Broadfoot et al., 1981a,b]; the same may be true of the upper atmosphere of Titan [Strobel and Shemansky, 1982]. Nevertheless, the emissions appear to be triggered by the deposition of solar energy since they are absent on the nightside of the planet and in the shadow of Saturn's rings [Broadfoot et al., 1981b]. Some of the ultraviolet observations of Saturn from Voyager have been reported previously [Broadfoot et al., 1981b; Sandel et al., 1982ba,b; Shemansky and Ajello, 1983; Smith et al., 1983]. Here, we present some newly analyzed data from Voyager 1 and 2 and further analysis of previously reported data.

In the following sections we present a variety of observations of the ultraviolet spectrum of Saturn from the Voyager 1 and 2 encounters. Much of the discussion centers on analysis of the limb profiles of H_2 band and hydrogen Lyman alpha intensities ($I(H_2)$ and I(Ly α) hereafter). The analysis of these data yields several rather surprising results. First, we find that above the homopause $I(H_2)$ and I(Ly α) are monotonically decreasing functions of altitude. This implies that there are emissions generated at low altitudes, near the homopause. Although $I(H_2)$ and I(Ly α) peak at low altitudes, the scale heights for the emissions are a factor of 5-10 larger than the scale height of the neutral atmosphere. Consequently, the source of excitation extends throughout the entire upper atmosphere from the homopause to well above the exobase.

Further, a radiative transfer calculation, based on the neutral atmosphere of Smith et al. [1983] indicates that the observed I(Ly α) at the subsolar point is a factor of 3-4 larger than the intensity expected from scattering of solar Ly α, while the intensities on the limb are 4-5 times larger than the solar-scattered intensity. This implies that the remaining Ly α emissions are collisionally produced. Also, $I(H_2)$ and I(Ly α) show similar variations in all Voyager observations outside the auroral regions. Since the H_2 bands must be collisionally excited, this supports the contention that the majority of Ly α emissions are collisionally generated.

Finally, the Ly α limb profile shows marked limb brightening for impact parameters near the homopause. Because of the increase in column abundance, limb brightening is expected for optically thin emissions, but Ly α is optically thick (the optical depth is ~10^5 on the limb) and should display limb darkening rather than brightening. We interpret this as evidence for proton or H atom precipitation because Ly α photons from this source have large doppler shifts and will escape the atmosphere without scattering; consequently, these Ly α emissions are optically thin and may explain the observed limb brightening. The center-to-limb variation, however, suggests that the Ly α emissions are a mix of optically thin and optically thick components. We estimate that the optically thin Ly α emission comprises ~15% of the observed disc brightness, when corrected to the zenith.

Discussions of upper atmospheric phenomena are often unnecessarily confused by a variety of conventions concerning height scales. This is especially true of Saturn because of its oblateness. In the following discussion we have adopted radius (i.e., distance from the center of the planet) as the basic measure of position in the upper atmosphere. To clarify the following discussion and facilitate comparison with other work, Table 1 lists the conversion between radius and some of the other scales commonly in use.

2. Observations

The Voyager Ultraviolet Spectrometer (UVS) has been described in detail elsewhere [Broadfoot et al., 1977, 1981a]; only its general characteristics are summarized here. The UVS is an objective grating spectrometer covering the wavelength range 500-1700 Å in 126 contiguous

Paper number 5A8310.
0148-0227/86/005A-8310$05.00

TABLE 1. Altitude Scales

Radius,[a] km	Altitude, km	Density column, cm^{-2}	Pressure, bars
58,700	0	-	1
59,500	800	2.48×10^{20}	8.0×10^{-7}
59,680[b]	980	1.26×10^{19}	4.1×10^{-8}
60,000	1300	8.20×10^{17}	2.6×10^{-9}
60,500	1800	7.08×10^{16}	2.3×10^{-10}
61,000	2300	6.20×10^{15}	2.0×10^{-11}
61,200[c]	2500	2.48×10^{15}	8.0×10^{-12}

[a] The radius used here is appropriate for the latitude of the V2 limb drift.
[b] Location of the homopause.
[c] Location of the exobase.

channels. Spectral resolution is approximately 30 Å and the slit size is 0.1° by 0.86°.

2.1. Limb Drifts

Bright limb drifts on both Voyager 1 and Voyager 2 (V1 and V2) examined the vertical structure of Saturn's atmosphere. In conjunction with occultation experiments, which probe the atmosphere through the absorption of stellar or solar radiation [Smith et al., 1983], the limb observations provide information on ionospheric or other processes capable of supplying the necessary energy to excite ultraviolet emissions.

The geometry relevant to the V2 bright limb observations is illustrated in Figure 1. The observations were made 7 hours before closest approach and lasted ~20 min. The planetocentric distance was 450,000 km. The UVS slit had an area projected onto the planet of 450 km by 38,700 km. The slit was tangent to the bright limb and the drift radial. The tangent point of the 1-bar level was at 27° S latitude and the solar zenith angle was 36°, corresponding to a local time of 1 hour and 40 min before noon.

The V1 observation geometry is similar. The observations occurred 2 hours and 30 min before closest approach at a planetocentric distance of 260,000 km. The first limb drift lasted 10 min and the second lasted 20 min. Again the drift was in the radial direction and occurred at 9.4° N latitude. The solar zenith angles for the first and second V1 drifts are 7.2° and 5.8° corresponding to local times of 24 min and 17 min before noon.

A basic problem in the interpretation of limb drifts is the determination of an accurate altitude scale. For the Voyager observations the spacecraft velocity determines the relative distance between two points in the limb drift, but the absolute scale is more difficult to determine. The V2 observations, however, were designed to immediately precede the δ-Sco entrance occultation. In effect, the limb drift was executed twice, once with and once without the star in the field of view. This provides a natural way to determine the altitude scale relative to the homopause. As described in detail by Smith et al. [1983], the neutral atmosphere will absorb starlight in the spectral regions where the absorption cross sections for the atmospheric constituents are large. Methane (CH_4), for example, has a large cross section in the 920–1106 Å region. The CH_4 density increases drastically at the homopause; consequently, the homopause is easily recognized in an occultation by the very abrupt onset of extinction of light in the 920–1106 Å region. This is shown in Figure 2a for the δ-Sco entrance occultation.

Figures 2b and 2c show the variations of $I(H_2)$ and I(Ly α) with impact parameter. $I(H_2)$ is determined by integrating the signal in the 920–1106 A region. Since there are substantial H_2 band emissions at longer wavelengths; this does not represent the total H_2 band intensity. We have corrected for this by multiplying the signal in the 920–1106 Å region by a constant to represent the total H_2 band intensity. If the H_2

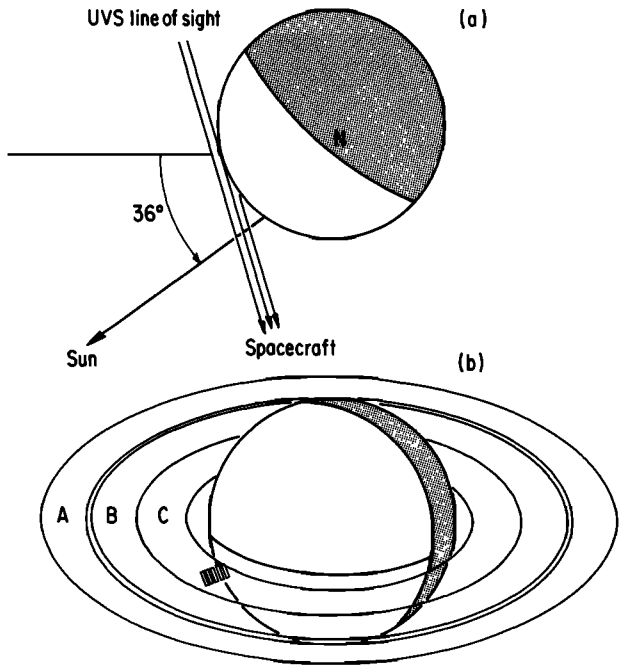

Fig. 1. (a) A north polar view of limb drift observation geometry. The three parallel lines indicate different UVS lines of sight during the drift. (b) A spacecraft view of the limb drift geometry. The relative sizes of the planet and UVS slit are approximately correct. Note that although the line of sight intersects the C ring, the optical depth of the ring is very small ($\tau < 0.01$) and should not affect the observation.

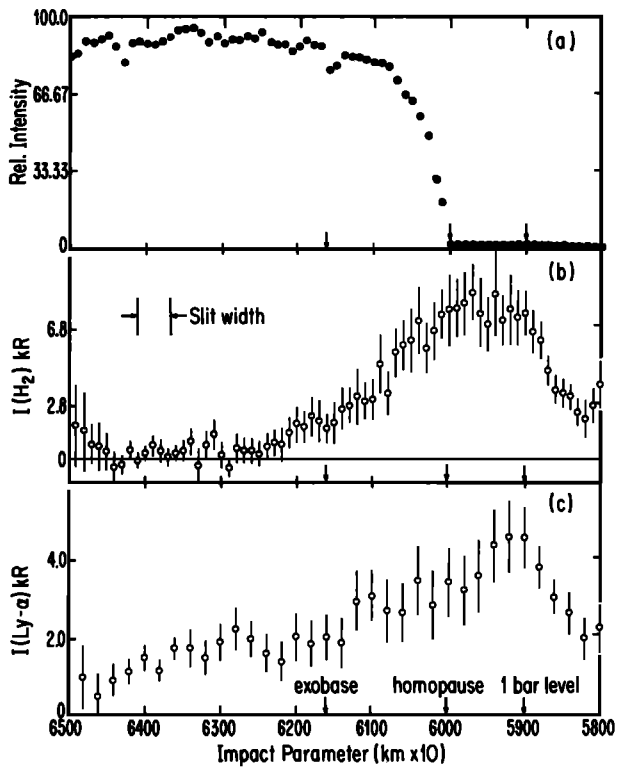

Fig. 2. (a) Absorption of light in the 920-1106 Å region from the δ-Sco entrance occultation. The very abrupt decrease at 60,000 km indicates the location of the homopuase. (b) The H_2 band signal between 920 Å and 1106 Å for the Voyager 2 limb drift. Note the large-scale height for the decrease of the emissions with altitude and the peak in intensity near the homopause. (c) The Ly α intensity for the V2 limb drift. Ly α also exhibits a very slow decrease with altitude and a peak at low altitude. The relative locations of the H_2 band and Ly α peaks are discussed further in the text.

band spectral shape varies, the proper scale factor may also vary, introducing errors into our determination of $I(H_2)$. Examination of the H_2 spectra suggests that these errors are rather small.

Data from the limb drifts on V1 are shown in Figures 3 and 4. The altitude scales were determined from images of the bright limb rather than an occultation measurement, but the relative locations of the emission peaks are consistent with the V2 altitude scale. The general features of the V1 limb drifts are very similar to the results from V2. Because of the more accurate altitude determination on V2 and the availability of a model for the neutral atmosphere derived from the V2 δ-Sco and solar occultations, we will concentrate on the V2 data. It is worth noting however, that I(Ly α) was approximately 30% greater at the V1 encounter than the V2 encounter, suggesting a decrease in the atmospheric atomic hydrogen content from the V1 encounter to the V2 encounter.

2.2. Latitude and Azimuthal Variations

The variations of the ultraviolet emissions with latitude and longitude were also studied by the Voyager UVS. A measurement of the latitudinal distribution of the emissions (Figure 5) shows no significant variations in either I(Ly α) or $I(H_2)$. The absence of variations in the apparent emission rates should not be interpreted as a lack of variation in the source of the emissions. In an optically thin atmosphere we would expect the brightness to increase roughly as the secant of the latitude if the source were a uniform thin layer. The lack of significant variation in I(Ly α) brightness could conceivably be attributed to optical thickness; however, $I(H_2)$ in Figure 5 is optically thin down to the level of the hydrocarbon homopause. The lack of variation in $I(H_2)$ therefore is interpreted as a declining source strength at higher latitudes. I(Ly α) does not show evidence of limb

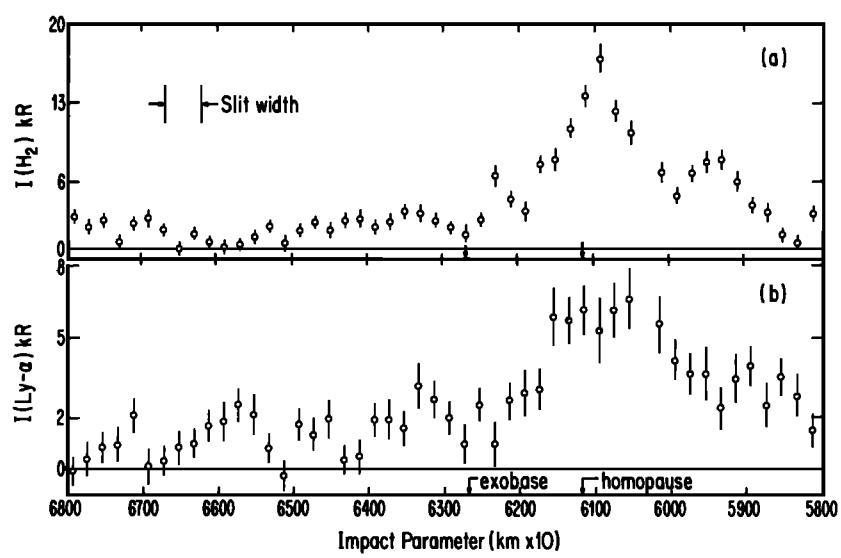

Fig. 3. (a) The H_2 band limb profile for the first Voyager 1 limb drift. (b) The Ly α limb profile for the first Voyager 1 limb drift. Note that the H_2 band peak and the Ly α peak are at approximately the same altitude.

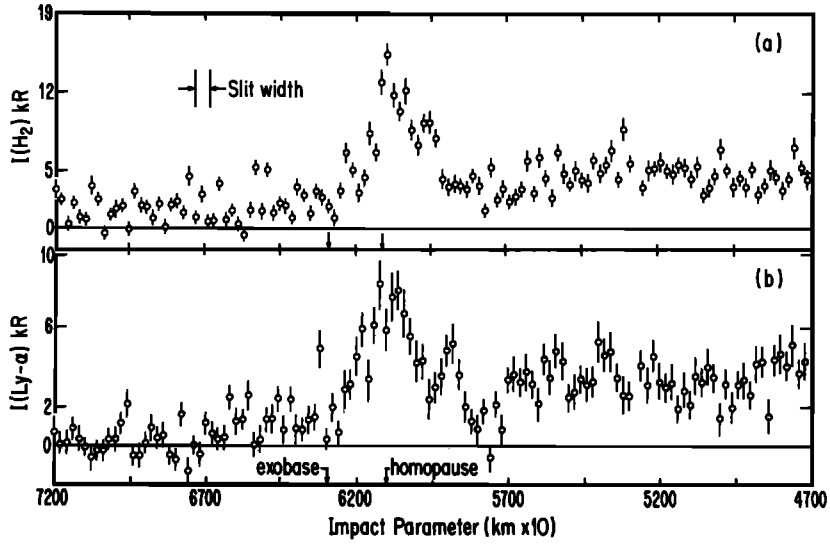

Fig. 4. (a) The H_2 band limb profile for the second Voyager 1 limb drfit. (b) The Ly α limb profile for the second Voyager 1 limb drift. Again the H_2 band and Ly α peaks are at the same altitude.

darkening, although limb darkening very near the pole (>80°N latitude) would be obscured by auroral emissions.

No discernible longitude-correlated variations have been detected in either the Ly α or H_2 band emissions from Saturn. To search for such an asymmetry, we have plotted in Figure 6 I(Ly α) and I(H_2) from a constant local time as Saturn rotated beneath the UVS slit. A similar observation on Jupiter resulted in the discovery of Jupiter's Ly α bulge [Sandel et al., 1980]. On Saturn, however, the intensities remain constant with longitude; this is not surprising considering the high degree of symmetry of Saturn's magnetic field. On the other hand, there are significant local time variations in I(Ly α) and I(H_2). Figure 7 shows that both I(Ly α) and I(H_2) decrease by approximately a factor of 2 from dawn to dusk. These measurements were made from V1, and a similar observation from V2 (containing fewer data points) shows very nearly the same behavior. This is precisely opposite in slope to the variation on Jupiter where the H_2 bands increase in brightness by a factor 2 from dawn to dusk [Shemansky, 1985, Figure 13]. The Ly α emissions from Jupiter, on the other hand, exhibit limb darkening in contrast to the limb brightening on Saturn, shown in Figure 7.

3. Modeling and Interpretation

Detailed modeling of the I(H_2) and I(Ly α) limb profiles are presented in the following subsections. However, many of the important features of the emissions can be seen directly in the data. First, the emissions appear to increase monotonically from above the exobase to the homopause, where they level off, then decrease as the line of sight moves onto the planet. The increase in intensity from high altitudes to the homopause suggests that there are emissions from all altitudes at and above the homopause. Because of strong CH_4 absorption for wavelengths less than 1350 Å, photons emitted from below the

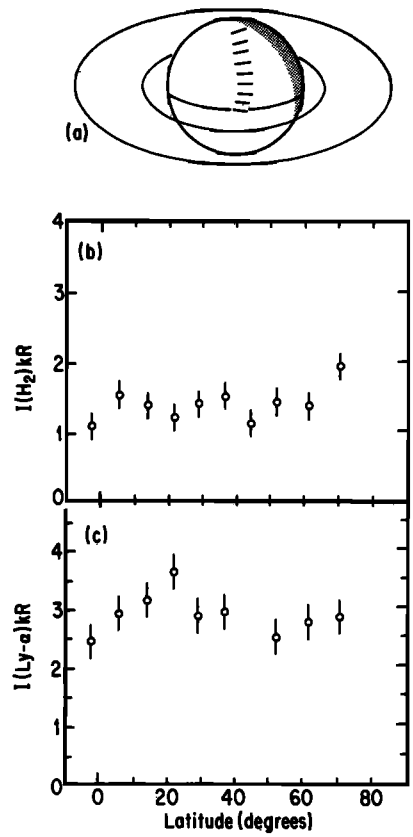

Fig. 5. (a) An illustration of the observation sequence for the data shown in Figures 5b and 5c. (b) The H_2 band emissions as a function of latitude. There is little variation, although the first point is rather low since it lies partially in the ring shadow. The last point is rather high because of contamination by auroral emissions. (c) The Ly α intensity as a function of latitude. Again there is little statistically significant variation.

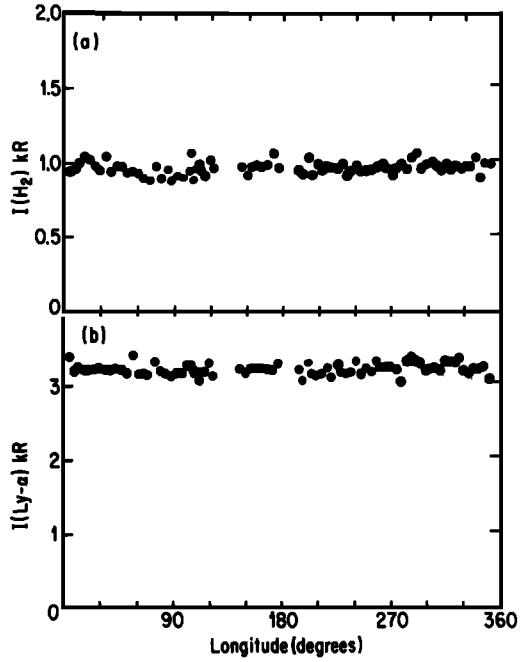

Fig. 6. (a) The H_2 band intensity as a function of Saturn longitude. There appear to be no significant zonal variations. (b) The Ly α intensity as a function of Saturn longitude. Again there are no apparent zonal variations.

homopause will be absorbed and, of course, undetected by the UVS. The homopause therefore defines the lower boundary of the region from which EUV emission in this spectral range may be observed. The decrease in intensity for impact parameters below the homopause is a natural consequence of the smaller column length for observations closer to the planet. The emissions appear to peak near the homopause, but both $I(H_2)$ and I(Ly α) have scale heights much larger than the scale height of the neutral atmosphere (~205 km [Smith et al., 1983]). This implies that although the emission brightness peaks at low altitudes, there are substantial emissions at very high altitudes. In other words, the excitation rate per neutral molecule is actually increasing with altitude.

As mentioned in the introduction, it is also surprising that I(Ly α) shows a distinct peak in roughly the same location as $I(H_2)$. This is surprising because the Ly α source is normally expected to be optically thick, while $I(H_2)$ is optically thin. The I(Ly α) and $I(H_2)$ profiles would be very different if, for example, most of the Ly α emissions resulted from scattering of solar Ly-α. We show in the next section that solar-scattered Ly α can account for only ~1 kR of the 4.5 kR of observed I(Ly α). In fact, $I(H_2)$ and I(Ly α) in the limb profiles as well as the latitude and azimuthal scans show remarkably similar variations. This is also partially true on Jupiter [Shemansky, 1985]; however, the correlation on Saturn appears even stronger, suggesting that $I(H_2)$ and I(Ly α) have a common collisional source.

There are some differences between the I(Ly α) and $I(H_2)$ limb profiles however. First, the I(Ly α) profile appears more extended than the $I(H_2)$ profile. This is probably due to the fact that resonantly scattered emissions from the sun and interstellar medium make up a significant fraction of the signal at high altitudes. Also, the density of atomic hydrogen relative to the H_2 density increases with altitude so any collisional source would produce proportionately more Ly α at high altitudes.

Another difference between the I(Ly α) profile and $I(H_2)$ profile occurs in the 59,000-km region where I(Ly α) appears to show a peak. As we pointed out in the discussion of the H_2 band profile, the apparent intensities should level off at the homopause then decrease as the column density decreased onto the planet. This may be evidence for a rather strong azimuthal or temporal variation in I(Ly α), but there is no indication of strong asymmetries in this small a longitude range (~10°) in any of the other data. Also the $I(H_2)$ limb profile is well fit by a spherically symmetric model, while we would expect to observe a similar effect if the overall source strength were varying either temporally or azimuthally. Finally, since the I(Ly α) limb

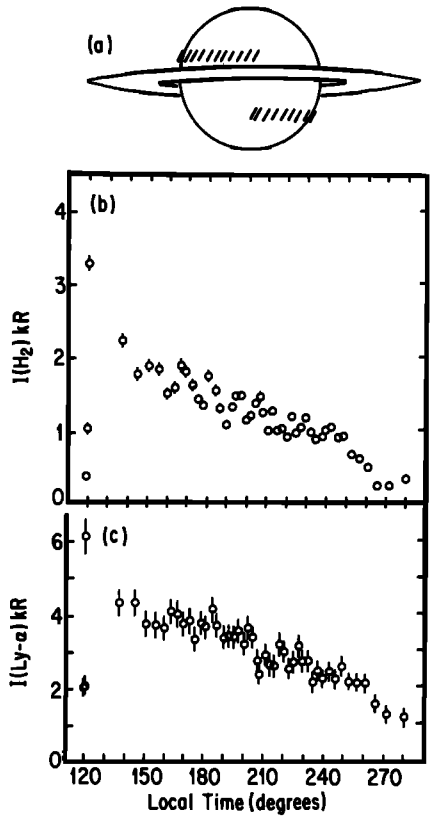

Fig. 7. (a) An illustration of the observation sequence designed to study local time behavior of the UV emissions. (b) The local time behavior of the H_2 band intensities. There is a factor of ~2 decrease from morning to evening. The high point near 120° is a result of the limb brightening discovered in the limb drift, and the low points above 260° indicate that the slit lies partly beyond the terminator. (c) The Ly α intensity as a function of local time. Again there is a factor of ~2 decrease from dawn to dusk as well as evidence of limb brightening and a decrease in intensity into the shadowed region.

profiles from the V1 limb drifts peak at the same altitude as $I(H_2)$, we are inclined to attribute the data points near 59,000 km to an artifact of the data analysis procedure. For example, at the resolution the Voyager UVS the Ly α line is superposed on a background of H_2 bands. At 59,000 km this background is larger than at higher altitudes, causing greater uncertainty in the background removal procedure. Further analysis of the complete spectrum may remove this difficulty; however, it is presently a source of uncertainity.

While the variations of the emissions with impact parameter evident in Figures 2, 3, and 4 indicate how the brightness varies with altitude, the UVS observation is really a line-of-sight measurement that must be inverted to yield the variation of emission rate with altitude. Rather than apply numerical inversion techniques to the data, we model the volume emission rate, adjusting the model to yield a limb profile which fits the data. An independent calculation, utilizing an inversion technique, found results very similar to those presented here (G. R. Smith, personal communication, 1985).

3.1. H_2 Emissions

To analyze the H_2 bands, we have converted the integrated intensity in the 920–1106 Å region to the total H_2 band intensity through comparison of the intensity determined by a fit of a synthetic spectrum to a disc spectrum with the 920–1106 Å intensity for the disc spectrum. Because of the short integration times on the limb drift it is impossible to determine the intensity for each limb drift point in this manner; therefore we have assumed that the conversion obtained for the disc is correct on the limb regardless of the H_2 foreground abundance. In reality, the conversion factor will vary because of resonant-scattering effects. However, the small albedo for scattering in this band system implies that multiple scattering is unlikely to play a significant role, and we estimate that the intensities that we have determined are accurate to better than 20%. Pure absorption by CH_4 is also included, by utilizing the CH_4 densities of Smith et al. [1983].

To model the H_2 emissions, we assume a simple exponential altitude dependence for the volume emission rate. Our level of knowledge at this point does not justify a more complex approach. However, a single scale height does not provide a good fit to the data. Spherical symmetry is assumed in this calculation, but departures from spherical symmetry will not seriously affect the accuracy of the result. The reason for this is twofold. The emission from a volume element along the line of sight will be weighted by the cosecant of the angle between the volume element, the planet's center, and the spacecraft; consequently, the emissions near the tangency point will be weighted most heavily. In addition, the emissions near the tangency point occur at the lowest altitude sampled for a given chord, and if the emissions increase with decreasing altitude, they will be more intense than the emission from other regions along the line of sight, again weighting the contribution from the tangency point most heavily. For these reasons we regard the altitude variation of the volume emission rate derived as representative for the region near the tangent point on the limb. Although deviations from spherical symmetry are clearly present, they should not seriously affect the accuracy of the volume emission rate for the location in question.

These arguments are not valid when the impact parameter is below the homopause since in that case the only emissions observed at and below 1216 Å are those which occur along the line of sight at altitudes above the homopause. Consequently, azimuthal asymmetries will be directly reflected in the data for impact parameters below 60,000 km (homopause) on the V2 limb drift. The difficulties this may cause in the interpretation of the data are offset by the fact that near the homopause a 1000-km difference in the altitude of the impact parameter implies a difference of only 10° in longitude. If azimuthal asymmetries are to affect the accuracy of the limb profile calculation then they must be significant in less than 20°. Further, we will present observational evidence that neither $I(H_2)$ or I(Ly α) vary significantly in this small a range.

Figure 8 shows $I(H_2)$ for the V2 limb drifts and the calculated limb profiles for three model volume emission rates. The corresponding volume emission rates are shown in Figure 9. Model B uses a single, large scale height (1500 km) and reproduces the data above 61500 km fairly well. Model A uses a much smaller scale height (200 km) and matches the data at smaller impact parameters. An improved fit results from the use of two scale heights in model C. Since the scale height of the neutral atmosphere also decreases at lower altitudes, this seems physically reasonable. These numerical results serve to quantify what is evident in the data, that the volume emission rates appear to increase with decreasing altitude into the homosphere and the emissions have very large scale heights (at high altitudes) implying a rising excitation and energy deposition rate per neutral molecule with increasing altitude, extending several scale heights into the exosphere.

There is no indication in the 920–1106 Å data that the emission rate decreases below the homopause. Preliminary analysis of the H_2 spectra over the full wavelength range (500–1700 Å), however, does not reveal the effects of hydrocarbon absorption suggesting that the emissions cannot extend more than a few scale heights into the homosphere.

3.2. Ly α Emissions

The determination of a volume emission rate for Ly α is more difficult because multiple-scattering effects must be considered. The situation is further complicated by the fact that part of the observed Ly α is due to the reflection of Ly α radiation from external sources (i.e., Ly α from the sun or interstellar medium). In fact, before the discovery of collisionally produced emissions from the outer planets it was generally assumed that the Ly α emissions arose only from solar scattering (see, for example, Wallace and Hunten [1973] or Yung and Strobel, [1980]). Under this assumption I(Ly α) could be used to determine the column

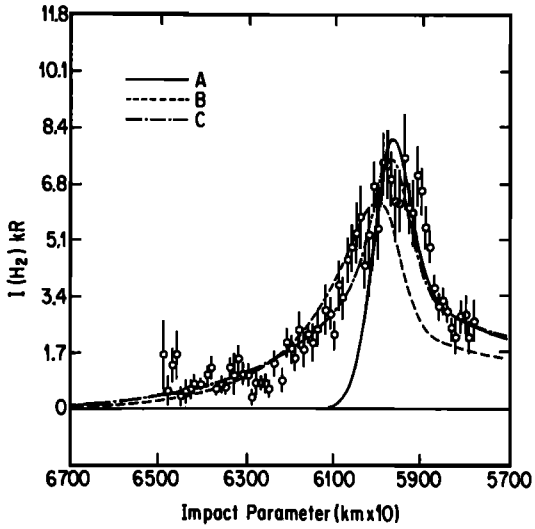

Fig. 8. The H_2 band limb profile along with model limb profiles. Models A, B, and C are shown in Figure 9 and explained further in the text.

abundance of hydrogen above the hydrocarbon homopause. However, the presence of collisionally produced H_2 band emissions and H Rydberg emissions [Shemansky and Ajello, 1983] implies that a significant fraction of the Ly α emissions must be due to collisions rather than resonant scattering. To model the limb drift, we must include both types of excitation, as discussed below.

3.3. Solar-Scattered Ly α

Calculation of the solar-scattered contribution is based on the model atmosphere determined from the UVS δ-Sco exit occultation and solar occultation experiments [Smith et al., 1983], a solar Ly α flux at 1 AU of 4.0×10^{11} photons cm^{-2} s^{-1} and the solar line shape of Vidal-Madjar [1977]. We treat the atmosphere as isothermal and plane parallel to calculate the source function but use spherical geometry in the calculation of the intensities. The results shown in Figure 10, curve A, demonstrate that the solar-scattered component is only a small fraction of the total Ly α intensity. Since there are local time variations in I(Ly α), it is possible that the hydrogen densitites appropriate at the limb drift may be larger than hydrogen densities derived from the δ-Sco exit occultation. If this is true, the solar-scattered component has been underestimated. Large variations seem unlikely since Saturn's rapid rotation should prevent the development of significant local time asymmetries in the neutral atmosphere. On the other hand, if the altitude distribution of atomic hydrogen does not change significantly with local time, then we expect a similar shape for the solar-scattered curve. In fact, we show below that an optically thick emission can not cause the limb brightening evident in the data. Consequently, the different shapes of the observed and solar-scattered limb profile constrain the possible amount of solar-scattered Ly α. Even if we take the extreme case by normalizing the solar-scattered curve to the intensity measured at high altitudes the measured intensity at the emission peak still exceeds the solar-scattered value by about 4 kR. A solar-scattered Ly α line moreover should show a cosinelike variation over the sunlit disc which is very unlike the observed behavior shown in Figure 5. We conclude that the majority of Ly α emissions seen on the limb are internally generated. Again, this is supported by the fact that the variations of I(Ly α) and $I(H_2)$ over the disk are similar, suggesting that they have a common collisional source.

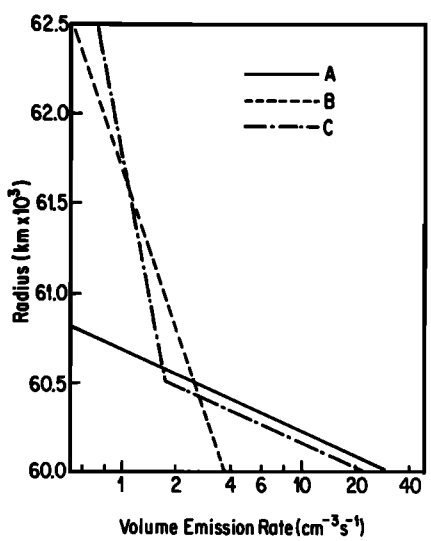

Fig. 9. The model volume emission rates used to calculate curves A, B, and C in Figure 8. Model B does not produce enough emission at high altitudes, while model A does not match the data at low altitudes. The best fit is obtained by a combination of scale heights in model C.

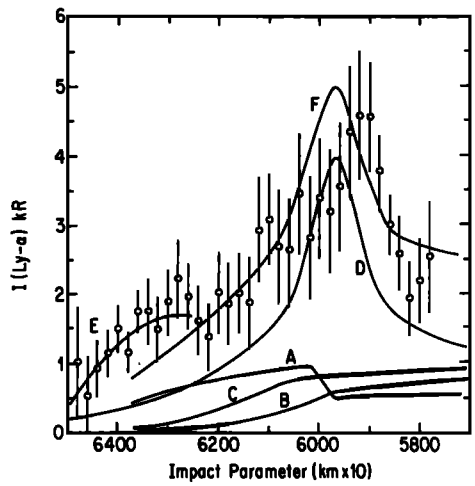

Fig. 10. The Ly α limb profile and model limb profiles. Curve A is the portion of the emissions due to solar reflection. Curves B and C are for internally generated Ly α emissions with source temperatures of 420 K and 60,000 K, respectively. Curve D is for optically thin emission. Curve E is an illustration of the Ly α intensity due to e + H. Curve F is the sum of curves A, B, and D.

TABLE 2. Excitation Cross Sections

	Reaction		Cross Section, 10^{-17} cm^2	Energy, keV
(R1)	$e+H \rightarrow$	$H(p)+e$	6.0	0.100
(R2)	$e+H_2 \rightarrow$	$H(2p)+H+e$	0.8	0.100
(R3)	$H^+ + H_2 \rightarrow$	$H(2p)+H_2^+$	5.0	10
(R4)	$H+H_2 \rightarrow$	$H(2p)+H_2$	4.0	10
(R5)	$e+H_2 \rightarrow$	$H_2(Ly+W_r)+e$	8.0	0.100

3.4. Collisionally Produced Ly α

The collisionally produced component of I(Ly α) may be caused by electron impact on atomic hydrogen, dissociative excitation of molecular hydrogen, or proton impact on either atomic or molecular hydrogen. Cross sections for these reactions at typical energies are listed in Table 2. The presence of H_2 band emissions implies that there will be some Ly α emissions from dissociative excitation of H_2. The amount of Ly α from this source may be estimated from I(H_2) (~7.6 kR at the peak of the limb profile). As shown in Table 2, the cross section for dissociative excitation of Ly α is much smaller than the cross section for H_2 band production. This is true for a wide range of electron energies [Ajello et al., 1984; Shemansky et al., 1985]. Taking a factor of 10 as the typical value for the ratio of the H_2 band to Ly α excitation cross sections, we estimate that at most, 700 R of the observed 4.5 kR may be due to dissociative excitation. This is an overestimate since multiple scattering will decrease the apparent intensity off the limb. Even this large a value, however, is only a small fraction of the observed 4.5 kR. Consequently, we rule out dissociative excitation as a possible source for the majority of the observed Ly α emissions.

Electron impact excitation of atomic hydrogen is also present to some degree in the emissions from the limb, and in fact, it may be the dominant contribution at altitudes above the exobase. The cross section for Ly α production from electron impact on H (R1) is similar to the cross section for H_2 band production from electron impact on H_2 (R2) at 100 eV. However, the mixing ratio of atomic hydrogen near the homopause is small ($[H]/[H_2] \sim 10^{-4}$), and we can expect a negligible contribution from electron impact on atomic hydrogen at this location. One further point is that the Ly α produced by atomic hydrogen would be characterized by the temperature of the neutral atmosphere. The limb profile from this source will be strongly affected by multiple scattering and, as we show later, the profile should not exhibit the limb brightening evident in the data.

Finally, it is possible that part of the Ly α emissions are due to energetic proton or H atom impact. At the proper energy a proton or H atom source will produce more Ly α emissions relative to the H_2 band emissions in accord with the observations on the limb. The Ly α emissions will be optically thin and capable of reproducing the observed limb brightening. Also, associated with energetic protons will be secondary electrons created in ionizing collisions with the neutral atmospheric constituents. The secondary electrons will excite H_2 band emissions supplying the observed correlation between I(H_2) and I(Ly α). For these reasons, energetic protons, rather than electrons, appear to be a likely source for the Ly α emissions at low altitudes.

3.5. Model I(Ly α) Limb Profiles

We can fortify the arguments given above by calculating model limb profiles for various source temperatures. To simplify the calculation, we assume that the Ly α volume emission rate has the same variation with altitude as the H_2 band volume emission rate. This will be true for the Ly α emissions produced by dissociative excitation and may be approximately correct for Ly α produced through proton impact on H_2. It will not properly account for the emissions from collisions with atomic hydrogen but will still serve to illuminate the character of the limb emissions.

The Ly α limb profile for source temperatures of 420 K and 60,000 K are shown as curves B and C in Figure 10. The procedure used to perform the radiative transfer calculations with a source temperature different from the atmospheric temperature is described in the appendix. Basically, a temperature of 60,000 K will enable more of the Ly α photons to escape the atmosphere without absorption than will a 420 K source temperature, but the calculations indicate that this is a small effect for the large column densities present in the limb observations. In other words, the self-absorption of Ly α is sufficiently strong to offset the increased column abundance off the limb and wash out an emission peak. This supports the argument that most of the Ly α emissions observed on the limb are not due to dissociative excitation of H_2 or electron excitation of H and must be produced by an optically thin source.

Because of the multiplicity of sources, the multiple-scattering effects, and the noise level in the data, it is impossible to accurately infer the altitude variation of each of the Ly α sources directly from the data. However, we can obtain some rough estimates from our knowledge of the atmosphere and the properties of the different sources. For example, in order to produce the limb brightening near the homopause the optically thin "hot" source must have substantial emissions at low altitudes. The limb profile for an optically thin emission is shown as curve D in Figure 10. We have assumed that the volume emission rate is proportional to the H_2 band volume emission rate. This should be approximately correct if the H_2 emissions are caused by secondary electrons associated with the hot source. Curve E is simply a hand-drawn estimate of the fraction of I(Ly α) due to electron collision with atomic H. This source can only be appreciable at high altitudes where the atomic H mixing ratio becomes large. Dissociative excitation of H_2 may contribute at low altitudes, but because of the small cross section, H_2 dissociation is unlikely to supply many photons. Solar-scattered Ly α, shown as curve A, also contributes at high altitudes.

We can gain further insight into the nature of the Ly α emissions and their approximate

TABLE 3. Analysis of UVS Disc Spectra

Emission	V1,[a] kR	V2, kR
I(Ly α) total	4.9	3.0
(source)		
$e + H \rightarrow H(2P)$	1.28	0.73
(apparent)		
$e + H \rightarrow H(Ly\ \alpha)$	2.2	1.00
(source)		
$e + H_2 \rightarrow H(2P)$	0.09	0.11
(apparent)		
$e + H_2 \rightarrow H(Ly\ \alpha)$	0.15	0.23
(apparent)		
$h_\nu + H \rightarrow H(Ly\ \alpha)$	~1.9	1.2
Total accounted emission	4.3	3.0
Excess (unaccounted)	0.6	0.4
$H_2(Ly + {}^{W}r)$	0.92	1.08
He 584	0.0024	0.0045
$\frac{I(Ly\ \alpha)}{I(H_2)}$	5.3	2.8
I(Ly β)	0.010	0.011

[a] We describe the source quantities, i.e., the altitude integral of the volume emission rate, in rayleighs to facilitate comparison with the apparent emission rate. The reader should bear in mind, however, that in general, the source rates and apparent emission rates differ because of absorption and multiple scattering.

distribution with altitude by examining the center-to-limb variation of $I(H_2)$ and I(Ly α). Comparison of $I(H_2)$ from Figure 7 and Figure 2 shows roughly a factor of 7 increase from the center of the disc to the peak of the limb profile (note that the data in Figure 7 are from V1, but the V2 values are similar). I(Ly α), on the other hand, increases by only 50%. This difference is most easily explained by assuming that the collisionally induced Ly α emissions are composed in part of a "hot," optically thin component (from proton or H atom precipitation) and a "cool," optically thick component (from electron excitation of H). On the disc, multiple-scattering effects will increase I(Ly α) by a factor of about 2 relative to optically thin emissions; while on the limb multiple scattering will depress I(Ly α) relative to optically thin emissions. The limb brightening of the "hot" source and the limb darkening of the "cool" source combine to produce the observed 50% disc-to-limb increase. The "hot," optically thick emissions therefore constitute only a fraction of the observed Ly α brightness.

To estimate the relative proportions of "hot" and "cool" emissions we assume that the optically thin Ly α emissions also increase by a factor of 7 from disc to limb. The amount of limb darkening for the "cool" source is difficult to estimate without an accurate model for the variation of volume emission rate with altitude. Because of the strong limb brightening, we should not be introducing large errors by assuming that the collisionally induced Ly α emission at the peak of the limb profile is due to the "hot" component. After subtracting 1 kR for the resonantly scattered sources and dividing by seven because of limb brightening we infer that ~500 R of the 3.5 kR seen on the disc are due to the "hot" Ly α source. Also, there should be about 1 kR of solar-scattered emission on the disc, leaving 2 kR from a collisional "cool" Ly α source, presumably electron excitation of atomic H with a small contribution from dissociative excitation of H_2. The "cool" Ly α emissions have been amplified by about a factor of 2 from resonant-scattering effects implying a column production rate of 1×10^9 photons cm^{-2} s^{-1} for the "cool" source compared to 5×10^8 photons cm^{-2} s^{-1} for the "hot" source and 1×10^9 photons cm^{-2} s^{-1} for the H_2 bands.

3.6. Disc Spectra

An alternate and complementary approach to determining the contribution of various sources to the EUV emission is through analysis of the EUV spectrum sampled by the Voyager UVS. This technique has been used extensively by Shemansky [1985] for the EUV emissions from Jupiter and by Shemansky and Ajello [1983] for the EUV spectrum of Saturn. The reader is referred to those works for an in-depth discussion of the procedure.

An inventory of inferred sources and apparent brightness of the various UV emissions for V1 and V2 sunlit disc observations is shown in Table 3. The Ly α source strength due to R1 has not been determined from I(Ly α) but rather has been inferred from the observed intensity of higher-lying members of the Lyman Rydberg series. (See Shemansky and Ajello [1983] for further details.) Because of multiple-scattering effects these values should be multiplied by approximately 1.7 to obtain the apparent brightness, listed below the source strength in Table 3. The R2 Ly α source is determined from the H_2 band brightness and has been modified by a similar radiative transfer calculation to obtain the apparent brightness. The solar-scattered contribution has been described earlier. The sum of Ly α intensities from solar scattering and electron impact sources is smaller than the observed signal. This discrepancy may be further evidence for the presence of a proton source, although it could also be due to accumulated errors in the other sources.

It is also possible to infer the foreground abundance of H and H_2 above the emitting regions of the atmosphere. Using this technique, it is possible to infer a weighted, mean altitude for the emissions. The V2 spectra imples an H foreground abundance of 3×10^{14} cm^{-2} and an H_2 foreground abundance of 3×10^{15} cm^{-2}, which roughly corresponds to the location of the exobase. The mean altitude of the H_2 volume emission rate determined from the limb drift is approximately 500–1000 km below the exobase. This difference is not surprising considering the different averaging procedures and remembering that the spectra are disc averages, while the limb drift is a measurement at a single location. (Preliminary examination of H_2 spectra suggest that the excitation altitude may vary in local time.)

3.7. Protons in an H_2 Atmosphere

If the UV emissions are due solely to energetic protons, through collisions with the

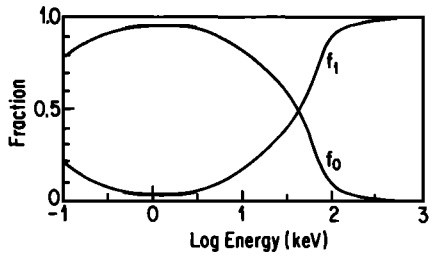

Fig. 11. The fractions of protons (f_1) and hydrogen atoms (f_0) in a equilibrated beam of protons and H atoms in an H_2 atmosphere as a function of energy. At low energies, hydrogen will dominate, while at high energies, protons will dominate.

primary particles and the effects of secondary electrons, then the relative intensities of the different UV emissions will constrain the energy of the protons. Consequently, we can address the feasibility of a proton source and the possible energy of the protons by examining the fate of a beam of protons in an H_2 atmosphere. The transport of protons through an N_2 atmosphere has been considered in some detail because of its importance in proton aurora [Van Zyl et al. 1984; Jasperse and Basu, 1982; Rees, 1982; Eather, 1967, and references therein]. The transport of protons through an H_2 atmosphere has received relatively little attention. One early attempt was made by Heaps et al. [1975] for applications to proton aurora on Jupiter. In general, calculations are hindered by the lack of reliable cross sections for many of the important reactions, making any calculation rather speculative. Nevertheless, in order to determine whether the relative intensities of the UV emissions are consistent with a proton source we consider some equilibrium calculations for energetic protons in an H_2 atmosphere.

Protons incident upon an H_2 atmosphere will quickly equilibrate into a mix of protons and H atoms. The relative proportions of protons and H atoms will be determined by the cross sections for stripping of H and electron capture by H^+. This is calculated for an equilibrated beam as a function of energy and is shown in Figure 11. Because H atoms are not constrained to travel along the nearly horizontal field lines, it is possible that the H atom/proton mix is not equilibrated until the collisional mean free path is smaller than the proton gyroradius. For a 10 keV proton this occurs at an H_2 density of $\sim 4 \times 10^9$ cm^{-3} corresponding to a planetocentric distance of 60,500 km. The results shown in Figure 10 are very similar to that for an N_2 atmosphere [Van Zyl et al., 1984]. At low energies the beam is mostly H, but at high energies, H^+ will dominate. Ly α emissions will, in general, result from the impact of both H^+ and H on H_2. The cross sections for this process have been measured by Dahlberg et al. [1968] and Birely and McNeal [1972]. Unfortunately, we were unable to find reliable measurements of the cross section for excitation of the Lyman and Werner bands by proton and H atom impact over the energy range of interest. At low energies, where the equilibrated beam is mostly H, the cross section for the Lyman bands from H on H_2 appears rather small [Dahlberg et al., 1968]. At high energies, on the other hand, the secondary electrons will dominate the emission process; consequently, we have ignored H_2 band production from H and H^+ impact in our calculations. To calculate the electron excited Ly α and H_2 band emission, we need the flux of secondary electrons (ϕ_e) which may be estimated from the H/H^+ flux (ϕ_{H/H^+}). We assume that the average energy expended in creating an electron–ion pair is 37 eV [Valentine and Currant, 1958] leaving the electron with 20 eV. We use the loss function for electrons in H_2 at this energy from Miles et al. [1972] to calculate a stopping distance for the electrons. The stopping distance multiplied by the production rate of electrons gives an estimate of the secondary electron flux. The ratio of ϕ_e to ϕ_{H/H^+} is given as a function of H/H^+ energy in Table 4. Knowing the ratio of ϕ_e to the ϕ_{H/H^+} and the cross sections for excitation of Ly α and H_2 emissions from H_2 collisions with electrons, protons, and H atoms, we calculate the ratio of Ly α from the various sources to the associated H_2 emissions. The cross section for Ly α production from electron for impact on H_2 is taken from Shemansky et al. [1985], and the cross section for Ly α production from electron impact on H is taken from Burke et al. [1967]. The results are displayed in Table 5. The values in columns 1–3 are the ratios of Ly α and H_2 band source strengths. The values in column 4 have been converted to apparent brightness by multiplying the optically thick emissions by a factor of 2. While this value was calculated for emissions from the subspacecraft point, it should vary slowly over the disc, and its variation is probably less than other uncertainties in the calculation.

As Table 5 indicates, $I(Ly\ \alpha)/I(H_2)$ increases toward lower energies. The values in column 2 and 4 depend directly on the atomic hydrogen mixing ratio and could be significantly higher or lower depending on the altitude of excitation. Unfortunately, we can not make this correction without an accurate model for the transport of protons in a nearly horizontal B field. The decrease of $I(Ly\ \alpha)/I(H_2)$ at higher energies is due to the increasing dominanace of secondary electrons in the emission process. Based on this estimate, it seems that the protons must be of fairly low energy (<5 keV) to explain the $I(H_2)/I(Ly\ \alpha)$ ratio. It is worth noting that Van Zyl et al. [1984] find that in a N_2 atmosphere, the secondary electrons begin to dominate the emissions at higher energies, about 20 keV. This difference may be related to differences in the properties of N_2 and H_2 or may reflect approximations in our calculation.

TABLE 4. Radio of Electron Flux to H/H^+ Flux

Energy, keV	$\phi_e/\phi H/H^+$
0.1	5.5×10^{-3}
0.5	9.25
1.0	68.4
5.0	250
10.5	315
50.0	472
100.0	389
500.0	129

TABLE 5. Ly α to H_2 Band Intensity Ratios

Energy, keV	S(Ly α)[a]/S(H_2)	S(Ly α)[b]/S(H_2)	S(Ly α)[c]/S(H_2)	I(Ly α)[d]/I(H_2)	I(Ly α)/I(H_2) Observed
1.0	1.1×10^{-2}	0.49	2.9	4.0	2.5
5.0	9.5×10^{-3}	0.48	0.48	1.4	
10.0	1.0×10^{-2}	0.50	0.30	1.3	
50.0	1.0×10^{-2}	0.49	0.13	1.1	
100.0	1.0×10^{-2}	0.50	0.13	1.1	
1000.0	1.0×10^{-2}	0.50	0.12	1.1	

[a] Ly α produced by electron impact on H_2.
[b] Ly α produced by electron impact on H. For the purposes of illustration we assume an H mixing ratio of 100%.
[c] Ly α produced by H, H^+ impact on H_2, H.
[d] The total sum of source strengths 1-3 with a amplification factor of 2 used for columns 1 and 2.

The ratio of I(Ly α) to the Lβ intenstiy (I(Ly β)) will also constrain the possible energy of precipitating protons. I(Ly β) is difficult to measure precisely because it is strongly blended with the H_2 band emissions at the resolution of the Voyager instrument. From the limb-drift spectra we estimate an upper limit of 80 R for I(Ly β). Because the resonant-scattering albedo for Lβ is 0.88, Lβ from "cool" sources will be suppressed on the limb, and we interpret the 80 R as an upper limit on the "hot" source. The observed I(Ly α)/I(Ly β) ratio consequently has a lower limit of ~44. We know of no measurements for the cross section for Lβ production from H on H_2 collisions but for a rough estimate of the cross section we can use the n^{-3} scaling law. This implies an I(Ly α)/I(Ly β) ratio of ~ 8, much smaller than the observed ratio. The cross section for Lβ production from proton excitation has been measured to be $7.4 \pm 6.3 \times 10^{-19}$ at 50 keV [Knize et al., 1984], while the cross section for Ly α production at this energy is 9.7×10^{-17} [Birely and McNeal, 1972], giving a I(Ly α)/I(Ly β) ratio of ~120. Based on these rather uncertain cross sections it would seem that the H^+/H beam needs to be energetic enough so that the exciting particles are mostly protons to be consistent with the I(Ly α)/I(Ly β) ratio but not so energetic that secondary electrons dominate the emission process to be consistent with the I(H_2)/I(Ly α) ratio. Clearly, a more thorough treatment of proton transport is needed to address the feasibility of a proton source and the possible energy ranges. Finally, we wish to point out that energetic protons were considered a possible source for part of the Ly α emission from Jupiter's nightside [McConnell et al., 1980].

4. Discussion

For the purposes of discussion it is convenient to separate the questions raised by the EUV observations of Saturn into two distinct categories, the immediate cause of the emissions, e.g., proton or electron impact, and the energy source and controlling factors for the emissions, e.g., solar ionizing radiation or magnetospheric precipitation. This paper has focused largely on the first topic and the major results are listed below. Following this, we consider the more difficult question of the energy source and the controlling factors responsible for the emissions.

1. The emissions are much weakened or absent on the dark areas of the planet implying that they are solar controlled although solar EUV does not supply sufficient energy to cause the emissions [Broadfoot et al., 1981b].

2. The H_2 emissions have a scale height approximately 10 times that of the neutral atmosphere and extend from the homopause to well above the exobase.

3. An estimate of the solar-scattered Ly α contribution based on the neutral atmosphere of Smith et al. [1983] indicates that most of the Ly α emissions are internally generated. This is supported by the correlation of the I(Ly α) and I(H_2) local time variations.

4. A fraction of the Ly α emissions appear optically thin implying that part of the source has a high temperature. This in turn suggests that the excitation may be due to energetic protons or neutral hydrogen atoms.

5. There is a factor of 2 decrease in both I(Ly α) and I(H_2) from dawn to dusk. This is strictly a local time effect since there are no discernible zonal variations in these emissions.

6. There is no latitudinal variation in the apparent UV emission rate which implies a decrease in the source rate toward the poles.

Previous discussions of sources for Jovian and Saturnian EUV emissions have concentrated on two possibilities, photoelectron excitation and magnetospheric precipitation. The absence of H_2 band emissions on the shadowed regions of the planet strongly suggests that photoelectrons play a role, but it was recognized early on that the energy deposited by solar UV was insufficient to account for the intense H_2 band emissions [Broadfoot et al., 1981b]. This discrepancy is far outside of instrumental uncertainties and is not related to inaccuracies in cross-section data. In fact, recent results [Shemansky et al., 1985] have revised the H_2 band cross sections downward by 40%, widening the discrepancy between UV emissions expected from photoelectron excitation and that observed.

Photoelectrons could still be the agent responsible for the UV emissions if there were a process (electric fields, for example) which

supplied additional energy to the photoelectrons. Unfortunately, this suggestion suffers from several difficulties. First of all, the H_2 band emission rate from photoelectron impact should peak in a narrow range of altitude centered about 2000 km above 1 bar (i.e., 60,500 km planetocentric distance at the latitude of the V2 limb drift) [Waite, 1981]. While electric fields could alter the altitude distribution of the emissions, it seems unlikely that photoelectrons could be responsible for the emissions near the homopause. As discussed earlier, the H_2 band volume emission rate peaks in the homopause region, and the very large density there should damp any acceleration mechanism. This strongly suggests that the emissions from the homopause region reflect local energy deposition. Furthermore, it seems unlikely that protons of ionospheric origin could be accelerated to sufficient energy to cause the optically thin emissions seen on the limb.

Magnetospheric precipitation remains a possibility; however, it must be triggered by solar radiation to explain the lack of emission from the shadowed region of the planet. In fact, the magnetosphere is the only plausible source of the energetic protons or H atoms which produce the optically thin emission seen on the limb. Upon further examination, however, magnetospheric precipitation also suffers from many difficulties.

The Saturnian magnetosphere is certainly a copious source of charged particles which may precipitate into the upper atmosphere (see Krimigis et al. [1983] for a discussion of the charged particle populations). For example, the charged particle densities in the L = 5-7 regions imply an energy deposition rate of 0.04 ergs cm^{-2} s^{-1}, assuming that precipitation occurs at one tenth the strong diffusion limit and protons as the major species [Krimigis et al., 1983]; (see also Cheng [1984]). This is nearly equal to the energy radiated in the EUV. We must bear in mind, however, that regions of the magnetosphere outside L=4 are magnetically connected to latitudes above 60° and this is where the bulk of precipitation should occur. Conventional, polar aurora are indeed observed on Saturn at latitudes near 80° [Sandel and Broadfoot, 1981], but this is a separate phenomenon from the one considered here. Charged particle densities at small L shells are unknown, but magnetic field lines which are connected to latitudes below 45° will also intersect the ring plane, which should efficiently absorb charged particles. Therefore magnetospheric precipitation at low latitudes must be the result of cross-field diffusion and must evade absorption in the rings.

Perhaps more disturbing than the difficulties of producing magnetospheric precipitation at low latitudes is the fact that there is no clear latitudinal signature of such a process in the EUV emissions. For example, charged particles traveling on field lines close to the equator should deposit their energy at higher altitudes than charged particles at high latitudes. This implies a decrease in the I (Ly α)/I(H_2) ratio with increasing latitude, but the observations show a constant ratio. Also, we would expect an inerease in brightness above 45° because of ring absorption at lower latitudes, but again no change is observed. We would like to point out that the difficulties of cross-field diffusion and ring-plane absorption can be avoided by postulating H atoms rather than protons as the primary particle in the precipitation process. The difficulty with this suggestion is in imagining an adequate source of fast H atoms which would preferentially cause precipitation on the dayside of the planet. In short, the characteristics of the EUV emissions suggest a process more complex than has been considered to date. Although many of the points made in the discussion above need to be examined with more comprehensive calculations, it seems apparent that the rather simple mechanisms considered so far are unable to explain the unusual morphology of the EUV emissions.

Regardless of the underlying source of the emissions, their existence implies significant perturbations of the ionosphere and neutral atmosphere. For example, besides exciting the UV emissions the energetic protons and electrons will heat the thermosphere. Smith et al. [1983] argue that the energy source of the UV emissions is probably also responsible for the high thermospheric temperature (420 K). Also, the scale height of the H_2 emissions implies a unusual temperature profile. Specifically, since the H_2 emissions extend to high altitude, we would expect a positive temperature gradient throughout the upper atmosphere. This question needs to be addressed further but is outside the scope of the paper.

It also seems likely that the source of the UV emissions may significantly affect the ionosphere. In fact, the electron density determined from radio occultation measurements shows a peak at high altitudes [Lindal, et al.,1985], and it seems likely that this may be associated with the high altitudes of the UV emissions. The H_2 band volume emission rate at the exobase is approximately 2 photons cm^{-3} s^{-1} (model C). The reaction efficiencies for H_2 band excitation and ionization by electron impact are given as a function of electron energy by Shemansky [1985]. At T_e = 300,000 K, for example, the ionization efficiency is about equal to the band excitation efficiency so we might expect an ionization rate of roughly 2 cm^{-3} s^{-1}. This is much larger than the ionization rate due to photoelectrons [Waite, 1981] and must be considered in ionospheric modeling calculations [Shemansky, 1985]. An equally important point concerns a possible depletion mechanism for the ionosphere. It was first pointed out by McElroy [1973] that the reaction

$$H^+ + H_2 \rightarrow H_2^+ + H \qquad (R6)$$

becomes energetically allowed for H_2 in a vibrationally excited state ($v'' \geq 4$). Since the lifetime of H_2^+ is much shorter than H^+, reaction (R6) decreases the ionospheric electron density. The intense UV emissions from high altitudes suggest that significant vibrational distributions of H_2 may develop; consequently, reaction (R6) may be operating and may partially explain the low ionospheric electron densities.

5. Summary

From the discussion above it is clear that further detailed modeling is needed to understand

the observed EUV emissions in terms of basic processes. Particular attention needs to be given to the problem of electron and proton transport in the nearly horizontal magnetic field near the equator and to the question of ring absorption. This paper has been largely concerned with a phenomenological description of the emissions and those attributes which may be directly inferred from the data. To this end we have called attention to several new aspects of the long-standing problem of finding an energy source for the intense, dayside EUV emissions from Saturn. This energy source must be capable of causing the very large scale heights of the EUV emissions and the limb brightening in both the Ly α and H_2 band emissions. We have interpreted the Ly α limb brightening as evidence that the emissions are optically thin, which, in turn, suggests protons or H atoms as the exciting particles. Because of the unusual character of the EUV emissions, we are unable to arrive at a satisfactory explanation of the EUV emissions either in terms of photoelectron excitation or simple, magnetospheric precipitation. These questions require further examination, employing more sophisticated transport calculations. Finally, the observed EUV emissions from high altitudes imply significant perturbations of the neutral atmosphere and ionosphere.

Appendix

The problem of radiative transfer with temperature differences between the emitting and absorbing atoms arises in many different contexts. Examples are the scattering of a solar emission line from a planetary atmosphere or multiple scattering in a nonisothermal atmosphere. A problem similar to the one considered here but for small scattering albedos has been discussed by Wallace and Hunten [1968] in reference to oxygen A band emission in the earth's atmosphere. We are unaware, however, of any published treatment valid for arbitrary temperature differences and large optical depths therefore the procedure used in the calculation is presented below. The calculations described are for an isothermal, plane-parallel atmosphere; however, extension to more complicated cases is straightforward.

To perform the radiative transfer calculation with a source temperature different from the atmospheric temperature we break the problem into two parts. From the primary source we calculate the singly-scattered radiation field taking into account the difference in temperature between the emitting and absorbing atoms. From the singly-scattered radiation field we calculate the source function assuming a plane-parallel, isothermal atmosphere. In keeping with the assumption of complete frequency redistribution, we assume that the radiation field is described by the atmospheric temperature after one scattering. The intensity is calculated as the sum of contributions from the primary source and the multiply-scattered source. In the calculation of the the primary source contribution we again take into account the difference in temperatures between emitting and absorbing atoms.

The basic equations of radiative transfer in a plane-parallel atmosphere, assuming complete frequency redistribution, are

$$S(\tau)= S_0(\tau) + \tilde{\omega} \int_0^{\tau_0} S(\tau')\, H\,(\tau-\tau')\, d\tau' \qquad (1)$$

and

$$4\pi I(\mu) = \tilde{\omega} \int_0^{\tau_0} S(\tau')\, T\,(\frac{\tau-\tau'}{\mu})\, d\tau' \qquad (2)$$

(see for example, Carlson and Judge [1971]) where the Holstein function, $T(\tau)$, is the rate of absorption per unit optical path length and $H(\tau,\tau')$ is the rate of absorption at τ' for photons emitted at τ. We also make use of the functions $G(\tau,\tau')$ and $V(\tau,\tau')$ defined through

$$H(\tau,\tau') = \frac{\partial G(\tau,\tau')}{\partial \tau'} \qquad \tau > \tau'$$

$$H(\tau,\tau') = -\frac{\partial G(\tau,\tau')}{\partial \tau'} \qquad \tau < \tau' \qquad (3)$$

and

$$V(\tau,\tau') = \frac{\partial H(\tau,\tau')}{\partial \tau'} \qquad \tau > \tau'$$

$$V(\tau,\tau') = -\frac{\partial H(\tau,\tau')}{\partial \tau'} \qquad \tau < \tau' \qquad (4)$$

In general, the expressions for $T(\tau)$, $G(\tau,\tau')$, $H(\tau,\tau')$, and $V(\tau,\tau')$ are

$$T\,(\frac{\tau-\tau'}{\mu}\,,r)=\frac{1}{\pi}\int_0^{\tau_0} \phi^*(x,B)$$

$$\exp\left[\frac{\tau-\tau'}{\mu}\cdot\phi(x,A)\right] dx \qquad (5)$$

$$H(\tau-\tau',r)+\frac{1}{\pi}\int_0^{\tau_0} \phi^*(x,B)\phi(x,A)$$

$$E_1\,[\,|\tau-\tau'|\cdot\phi(x,A)]\,dx \qquad (6)$$

$$G(\tau-\tau',r)=\frac{1}{2\pi}\int_{-\infty}^{\infty} \phi^*(x,B)$$

$$E_2\,[\,|\tau-\tau'|\cdot\phi\,(x,A)]\,dx \qquad (7)$$

$$V(\tau-\tau',r)=\frac{1}{2\pi}\int_{-\infty}^{\infty} \frac{\phi^*(x,B)}{\phi(x,A)}\cdot$$

$$\left[E_3\,[\,|\tau-\tau'|\cdot\phi(x,A)] - \frac{1}{2}\right] dx \qquad (8)$$

where x is the frequency of the radiation in units of the Doppler width, determined by the atmospheric temperature. $\phi(x,A)$ and $\phi^*(x,B)$ are the line profiles corresponding to the atmospheric and source temperatures respectively. For the calculations presented here we use Voight functions; A and B are the appropriate Voight parameters. The relationship between $\phi(x,A)$ and

$\phi^*(x,B)$ is determined by r, the ratio of atmospheric to source temperature.

$$\phi^*(x,B) = r \cdot \phi(r \cdot x, r \cdot A) \quad (9)$$

The multiply-scattered source, $S(\tau)$, is calculated from,

$$S_1(\tau)=\tilde{w}\int_0^{\tau_0} S_0(\tau)H(\tau-\tau', r)\, d\tau' \quad (10)$$

and

$$S(\tau)=S_1(\tau)+\tilde{w}\int_0^{\tau_0} S(\tau)\, H(\tau-\tau',1)\, d\tau' \quad (11)$$

The intensity due to the multiply-scattered source is given by

$$4\pi\, I_1(\mu)=\tilde{w}\int_0^{\tau_0} S(\tau')\, T\left(\frac{\tau-\tau'}{\mu},1\right) d\tau' \quad (12)$$

and the intensity due to the primary source is given by

$$4\pi\, I_0(\mu)=\tilde{w}\int_0^{\tau_0} S_0(\tau')\, T\left(\frac{\tau-\tau'}{\mu}, r\right) d\tau' \quad (13)$$

The total intensity is, of course,

$$I(\mu) = I_1(\mu) + I_0(\mu)$$

To perform the radiative-transfer calculation we transform the integral equations (1) and (2) into matrix equations by partitioning the atmosphere into zones of varying thickness. To partition the atmosphere efficiently, we require that the primary source function, $S_0(\tau)$ at the center of each zone, may be interpolated from the values at the boundaries of the zone to a specified accuracy (typically 1%). The source function is then assumed to vary linearly in each zone, and the equations are solved using the technique described by Strickland and Rees [1974].

Acknowledgments. We would like to acknowledge many helpful discussions with G. R. Smith and J. Holberg and to thank A. L. Broadfoot and D. M. Hunten for critical readings of the manuscript. M. Fitzgibbon provided much valuable support in Voyager data reduction. This work was partially supported by NASA grant NAGW-610 to the University of Arizona.

The Editor thanks the J. H. Waite, Jr. and a second referee for their assistance in evaluating this paper.

References

Ajello, J. M., D. E. Shemansky, T. L. Kwok, and Y. L. Yung, Studies of extreme-ultraviolet emission from Rydberg series of H_2 by electron impact, Phys. Rev. A, 29, 636, 1984.

Birely, J. H., and R. J. McNeal, Formation of H(2p) and H(2s) in collisions of protons and hydrogen atoms with hydrogen molecules, Phys. Rev. A, 5, 692, 1972.

Broadfoot, A. L., et al., Ultraviolet spectrometer experiment for the Voyager mission, Space Sci. Rev., 21, 183, 1977.

Broadfoot, A. L., et al., Overview of the Voyager ultraviolet spectrometry results through Jupiter encounter, J. Geophys. Res., 86, 8259, 1981a.

Broadfoot, A. L., et al., Extreme ultraviolet observations from Voyager 1 encounter with Saturn, Science, 212, 206, 1981b.

Burke, R. G., A. J. Taylor, and S. Ormonde, Low-energy electron scattering by atomic hydrogen, III, Comparison of theory and experiment for electron induced excitation of hydrogen to the N=2 level, Proc. Phys. Soc., 92, 345, 1967.

Carlson, R. W., and D. L. Judge, The extreme ultraviolet dayglow of Jupiter, Planet Space Sci., 19, 327, 1971.

Cheng, A. F., Magnetospheres, rings, and moons of Uranus, Uranus and Neptune, edited by J. Bergstalh, NASA Conf. Publ., 2330, J. Bergstalh, 557,1984.

Dahlberg, D. A., D. K. Anderson, and I. E. Dayton, Vacuum ultraviolet emission by proton and H-atom impact on H_2, Phys. Rev., 170, 127, 1968.

Eather, R. H., Auroral proton precipitation and hydrogen emissions, Rev. Geophys., 5, 207, 1967.

Heaps, M. G., B. C. Edgar, and E. S. Green, Jovian proton aurora, Icarus, 24, 78, 122, 1968.

Jasperse, J. R., and B. Basu, Transport theoretic solution for auroral proton and H atom fluxes and related quantities, J. Geophys. Res., 78, 1975.

Knize, R. J., S. R. Lundun, and F. M. Pipkin, Measurement of excited state charge exchange reactions, Phys. Rev. A, 29, 1114, 1984.

Krimigis, S. M., J. F. Carbary, E. P. Keath, T. P. Armstrong, L. J. Lanzerotti, and G. Gloeckler, General characteristics of hot plasma and energetic particles in the Saturnian magnetosphere: Results from the Voyager spacecraft, J. Geophys. Res., 88, 8871, 1983.

Lindal, G. F., D. N. Sweetnam, and V. R. Eshleman, The atmosphere of Saturn: An analysis of the Voyager radio occultation measurements, The Astron. J., 90, 1136, 1985.

McConnell, J. C., B. R. Sandel, and A. L. Broadfoot, Airglow from Jupiter's nightside and crescent: Ultraviolet spectrometer observations from Voyager 2, Icarus, 43, 129, 1980.

McElroy, M. B., The ionospheres of the major planets, Space Sci. Rev., 14, 460, 1973.

Miles, W. T., R. Thompson, and A. E. S. Green, Electron-impact cross sections and energy deposition in molecular hydrogen, J. Appl. Phys., 43, 678, 1972.

Rees, M. H., On the interaction of auroral protons with the earth's atmosphere, Planet. Space Sci., 30, 463, 1982.

Sandel, B. R., and A. L. Broadfoot, Morphology of Saturn's aurora, Nature, 292, 679, 1981.

Sandel, B. R., J. C. McConnell, and D. F. Strobel, Eddy diffusion at Saturn's homopause, Geophys. Res. Lett., 9, 1077, 1982b.

Sandel, B. R., et al., Extreme ultraviolet

observations from Voyager 2 encounter with Saturn, Science, 215, 548, 1982a.

Sandel, B. R., A. L. Broadfoot, and D. F. Strobel, Discovery of a longitudinal asymmetry in the H Lyman-alpha brightness of Jupiter, Geophys. Res. Lett., 7, 5, 1980.

Shemansky, D. E., An explanation for the H Ly α longitudinal asymmetry in the equatorial spectrum of Jupiter: An outcrop of paradoxical energy deposition in the exosphere, J. Geophys. Res., 90, 2673, 1985.

Shemansky, D. E., and J. M. Ajello, The Saturn spectrum in the EUV-Electron excited hydrogen, J. Geophys. Res., 88, 459, 1983.

Shemansky, D. E., J. M. Ajello, and D. T. Hall, Electron excitation of H_2: Rydberg band systems and the benchmark dissociative cross sections of H Ly α, Astrophys. J., 296, 765, 1985.

Smith, G. R., D. E. Shemansky, J. B. Holberg, A. L. Broadfoot, and B. R. Sandel, Saturn's upper atmosphere from the Voyager 2 EUV solar and stellar occultations, J. Geophys. Res., 88, 8667, 1983.

Strickland, D. J., and M. H. Rees, The O I λ 1304 and λ 1356 emissions in aurorae, Planet. Space Sci., 22, 465, 1974.

Strobel, D.F., and D.E. Shemansky, EUV emissions from Titan's upper atmosphere: Voyager 1 encounter, J. Geophys., Res., 87, 1361, 1982.

Valentine, J. M., and S. C. Curran, Average energy expenditure per ion pair in gasses and gas mixtures, Rep. Prog. Phys., 21, 1, 1958.

Van Zyl, B., M. W. Grealy, and H. Newmann, Prediction of photon yields for proton aurorae in an N_2 atmosphere, J. Geophys. Res., 89, 1701, 1984.

Vidal-Madjar, A., The solar spectrum at Lyman alpha 1216A, in The Solar Output and It's Variation, edited by O. R. White, Colorado Associated University Press, Boulder, Colo., 213, 1977.

Waite, J. H., The ionosphere of Saturn, Ph.d. thesis, Univ. of Mich. Ann Arbor, 1981.

Wallace, L., and D. M. Hunten, Dayglow of the oxygen A band, J. Geophys. Res., 73, 4813, 1968.

Wallace, L. and D. M. Hunten, The Lyman alpha albedo of jupiter, Astrophys. J., 182, 1013, 1973.

Yung, Y. L., and D. F. Strobel, Hydrocarbon photochemistry and Lyman alpha albedo of Jupiter, Astrophys. J., 239, 395, 1980.

S. Kumar, B. R. Sandel, D. E. Shemansky, and R. V. Yelle, Lunar and Planetary Laboratory, University of Arizona, Tucson, AZ 85721

(Received November 18, 1985;
revised April 23, 1986;
accepted April 25, 1986.)